High resolution non-contact AFM imaging of liquids condensed onto chemically nanopatterned surfaces

Antonio Checco[a,*], Yuguang Cai[b], Oleg Gang[c], Benjamin M. Ocko[b]

[a]Condensed Matter Physics and Materials Science Department, Brookhaven National Laboratory, Upton, NY 11973, USA
[b]Physics Department, Brookhaven National Laboratory, Upton, NY 11973, USA
[c]Center for Functional Nanomaterials, Brookhaven National Laboratory, Upton, NY 11973, USA

Abstract

The wetting of ethanol and octane on chemically nanopatterned surfaces has been investigated using Atomic Force Microscopy (AFM) under controlled environmental conditions. The patterns were generated on a methyl-terminated, organic monolayer using an AFM electro-oxidation process. The subsequent wetting of the organic liquids was studied using non-contact mode AFM under equilibrium conditions with the vapor. This study of condensed nanoliquids provides the first reliable measurements of sub 100 nm liquid profile shapes. The derived contact angles give an estimate of the line tension.
Published by Elsevier B.V.

1. Introduction

Scanning Probe Microscopy (SPM) is a powerful and versatile imaging technique which has been responsible for many of the recent scientific advances in the study of soft-matter [1,2] and biological interfaces [3–5]. Recently it has been shown that SPM is also capable of imaging thin liquid films and liquid droplets formed on solid supports [6–12]. Imaging liquid surfaces with SPM presents a special challenge compared to imaging solid and soft states of matter. Indeed, the proximity of the microscope tip with the liquid surface can induce either capillary wetting ("bridging") or strong perturbations of the liquid surface profile. The dynamics mode approach [13] overcomes the limitation of standard SPM methods. Here, an oscillating SPM cantilever/tip ensemble is used to probe the liquid surface at a working distance sufficiently far from the surface where long-range attractive forces are the dominant interaction.

Salmeron and coworkers [6,7] have imaged films and droplets of ionic liquids using a Polarization Force Microscope where a biased SPM tip interacts with the liquid surface through long-range electrostatic force. Luna et al. [8], Gil et al. [9] and Checco et al. [10,11] have shown that similar results can be achieved using even weaker forces such as van der Waals interactions (non-contact, amplitude modulation atomic force microscopy, AM-AFM [13]). Although the absence of tip-liquid contact is crucial for obtaining stable images of the liquid surface, in limited cases [12,14] it has been shown that it is possible to image droplets with the AM-AFM in the tapping mode [13], where the tip touches the liquid surface during each oscillation cycle. In this case, where a capillary meniscus between tip and liquid is formed and ruptured during each cycle, the imaging mechanism is not fully understood [12]. It should be noted that the wetting properties of the tip may play a significant role because they influence the size of the capillary meniscus on the tip and therefore the perturbation of the liquid surface [15].

In addition to the technical issues associated with imaging liquid surfaces with SPM, it is also important to

---

*Corresponding author. Tel.: +1 631 344 3319, fax: +1 631 344 2739.
E-mail address: checco@bnl.gov (A. Checco).

control and stabilize the liquid objects. This control is often obtained by adjusting the vapor pressure of the volatile liquid inside an enclosed chamber. In this manner, thin films [7–9] and even droplets [10,11] have been stabilized. In the present study, the scanning tip of the AFM and the sample are enclosed in a sealed chamber where the sample temperature is adjusted relative to the chamber temperature. This arrangement allows the chemical potential (therefore the condensation) of the liquid on the sample to be precisely controlled [38].

The above mentioned apparatus, in the non-contact AM-AFM mode, is used here to study liquid adsorption onto chemically nanopatterned surfaces. Our observations, in agreement with previous studies on homogeneous substrates [10,11], demonstrate that non-contact mode provides reliable information on the topography of liquids and that the transition to conventional tapping mode leads to serious sample deformation. Lateral resolution less than 10 nm is shown to be achievable with non-contact mode when ultra-fine tips are utilized. Although AFM has been used recently to study wetting on patterned surfaces [16,17], here we study for the first time the case of nanopatterns exposed to volatile liquids in equilibrium with a macroscopic vapor reservoir. Our results demonstrate that "wettable" carboxylic domains, nanopatterned onto a "non-wettable" methyl surface, are effective to confine liquids at the nanoscale. This enables the study of wetting phenomena in ultra-confined geometries. If water or aqueous solutions were to be used, biological phenomena could be investigated. Nanoliquid templating is also important for applications such as nanofluidics [18], whose purpose is to confine and guide ultra small quantities of liquids through designated regions of the substrate. These chemical patterned surfaces are also ideal substrates to study morphological wetting transitions [19–21], where neighboring lines merge together to form a single larger channel, and the relative role of the line tension, compared to the surface tension, in determining the profiles of liquid nanodrops [10]. In the following sections, we demonstrate the application of chemically patterned surfaces to investigate a range of nanoscale equilibrium wetting phenomena.

2. Experimental

The fabrication of the chemical patterns and the wetting experiments were conducted using a Pico Plus (Molecular Imaging) AFM which is contained in an environmental chamber compatible with saturated vapors of water and many organic liquids. The chemical patterns were prepared on Silicon (1 0 0) wafers (p doped, resistivity $< 100 \, \Omega \, cm$) passivated with a hydrophobic monolayer of octadecyltrichlorosilane molecules (OTS) according to standard procedures [23]. This self-assembled monolayer (SAM) exposes well-packed, methyl terminal groups as supported by the literature value of the water advancing contact angle of $110 \pm 1°$ measured on these substrates. AFM studies

carried out in topography mode showed the presence of a nearly defect free, well packed SAM. Using "local oxidation nanolithography" [23], the OTS terminated wafers were chemically nanopatterned by a process which electrochemically converts the terminal methyl group of the OTS into a carboxylic acid group. The important role of the humidity and the tip bias in this process has been recently studied in detail Ref. [24]. To fabricate the patterns a Ti–Pt coated silicon tip (MikroMasch type CSC17) was placed in contact with the OTS surface under constant ambient humidity which was adjusted within 1% by a homemade controller. By scanning the potential biased tip at constant speed, "carboxylic lines," composed of COOH terminated regions, could be written on the methyl surface, as illustrated in Fig. 1a. With a writing speed of 9 μm/s, a sample to tip bias of 8 V and 100% relative humidity "carboxylic lines" as small as 40 nm were created, as shown in Fig. 1b,c. The lines were readily visible in the friction mode image, as shown in Fig. 1c. In this mode the sensitivity to the chemical nature of the surface [25] is high whereas, a weak negative contrast ($\sim$2–3 Å), see Fig. 1b, is obtained in topography mode. This proves that the chemical patterning has a minimal effect on the geometric landscape [39].

Wetting studies of ethanol and octane on the chemical nanostripes were carried out using the same environmental
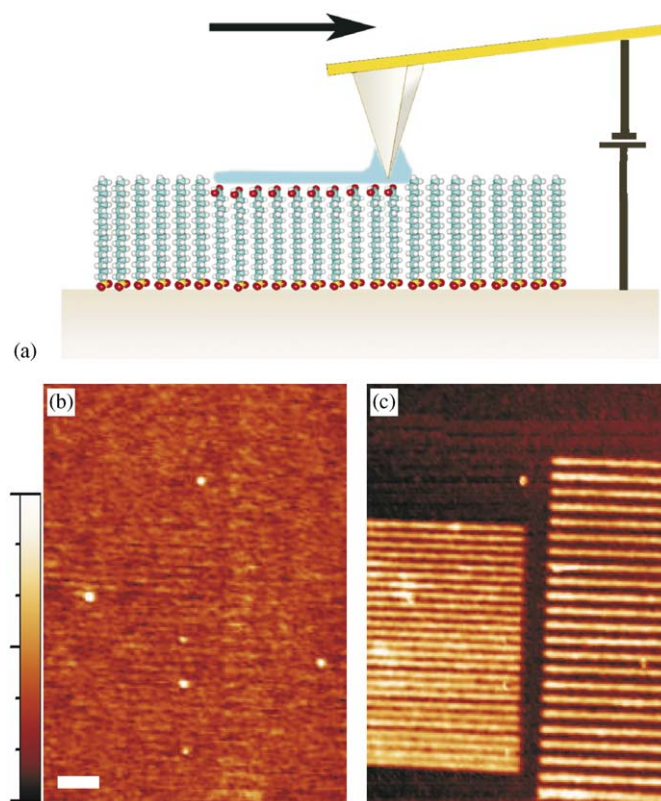

Fig. 1. (a) Schematics of the chemical patterning technique described in the text; (b) contact mode AFM image of an OTS surface patterned with COOH nanostripes (the lateral scale is 200 nm) and (c) corresponding friction force image.

AFM used in the patterning procedure detailed above. A reservoir of the organic liquids was introduced into the environmental AFM chamber. Afterwards, the chamber was flushed with nitrogen for 15 min to remove most of the water vapor. As detailed below, the organic liquids will selectively condense on the COOH terminated stripes. This observation is consistent with macroscopic studies that show that ethanol and octane completely wet a COOH terminated surface [26]. In contrast, these liquids do not wet the lower energy OTS surface. Rather, a finite advancing contact angle of $30 \pm 1°$ and $8 \pm 1°$ is observed in optical measurements respectively for ethanol and octane. Precise control of the amounts of deposited liquid is obtained by varying the substrate temperature relative to the environmental reservoir of the AFM by an amount ΔT. This is accomplished by heating or cooling the sample with a Peltier cooler/heater device where the reservoir temperature was kept at room temperature which was controlled at $25°C$. Multiple measurements on several samples were carried out to ensure that the measurements presented are representative.

Liquid topographies were imaged in non-contact AM-AFM, a dynamic imaging technique where the AFM cantilever is vibrated with a relatively small amplitude A_{fr} (1–10 nm) at a fixed frequency v_0 which is about 100 Hz higher than the fundamental cantilever resonance frequency (amplitude modulation technique [13], see Fig. 2a). When the sharp tip is brought sufficiently close to the surface the attractive van der Waals force shifts the resonant frequency of the tip oscillator towards lower frequencies. Since the lever is oscillating at v_0 this interaction causes the oscillating amplitude to decrease to $A_{sp} < A_{fr}$ (see Fig. 2a inset). The AFM is operated in a feedback mode so as to maintain a constant amplitude A_{sp} by adjusting the tip height. Under these conditions the tip height profile provides the topographical surface image.
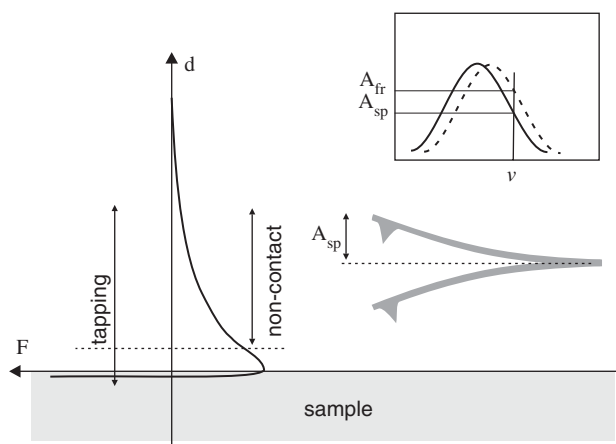

Fig. 2. Essential principles of dynamical AFM mode with amplitude modulation detection (inset). Depending on oscillation amplitude and distance of approach the cantilever/tip ensemble is maintained within the long range tail of the attractive surface potential (non-contact mode) or it can periodically experience short range repulsive forces (tapping mode).

However, the non-contact mode is maintained only for a range of A_{sp}. Decreasing A_{sp} moves the tip closer to the surface and this increases the resolution in both the vertical and lateral directions [27]. This also narrows the risk of accidental contact between the tip and sample. In this case the tip experiences additional adhesive and repulsive interactions which can drive the cantilever into the tapping mode [28–31] and this involves periodic contact between the tip and the surface. Our experience shows that a value of $A_{fr} \leqslant 10$ nm provides optimal non-contact imaging avoiding the transition to the tapping mode. It is equally important to use stiff cantilever beams which can oscillate close to the surface without becoming mechanically unstable. Such instabilities occur when the surface force gradient becomes larger than the cantilever's force constant. The typical force constant of the beams used is 40 N/m and the resonant frequency is about 300 kHz where the quality factor is about 500 (MikroMasch series NSC15 cantilevers). With these cantilevers, lateral resolutions of order 15 nm (slightly larger than the nominal tip radius) could be obtained in NC-AFM. To achieve better lateral resolution (between 7–10 nm) we have used similar cantilevers beams equipped with sharper tips having a curvature radius less than 5 nm (MikroMasch type HIRES DP15). The errors presented in the text for contact angles and the lateral dimensions of liquid nanostructures reflect the combined errors from many samples and many runs of the samples after fitting the profiles.

3. Results and discussion

AFM images of liquid ethanol coated nanostripes (80 nm wide) are shown in Fig. 3. In this picture, the slow scanning direction is from the bottom to the top and three different regions can be distinguished which are labelled A, B and C in the figure. Regions A and C correspond to the non-contact mode and region B corresponds to the tapping mode. In region A the stripes show a positive contrast of 2 nm compared to the methyl surface. This contrast originates from the thin liquid film adsorbed on the stripes. At the bottom of region B the amplitude A_{sp} is suddenly reduced (while the tip is scanned over the surface) and the topographic contrast associated with the liquid stripes is no longer apparent. At the bottom of region C the initial value of A_{sp} is restored and again the topographic contrast associated with the wet stripes has recovered. The transition between the different regions is due to the crossover between non-contact and tapping modes which occurs above and below a critical value of A_{sp}. In the IC case the tip penetrates through the liquid film and therefore only the hard solid substrate is imaged. The substrate appears flat because, as explained in the previous section, the carboxylic regions have a very small contrast compared to the methyl regions. The signature of this transition from one oscillation state to another is given by the large, negative jump of the phase lag between the resonator and the excitation [28–31]. This phase jump is illustrated in
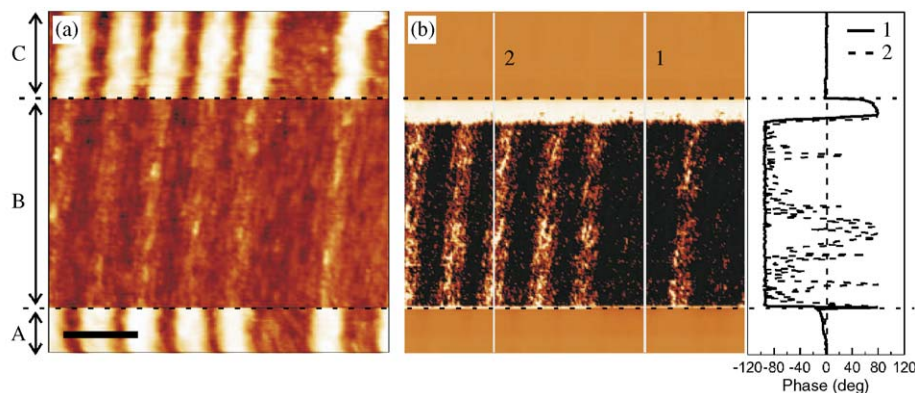
Fig. 3. (a) Topography and (b) phase signal on the "liquid nanostripes" change drastically as the setpoint amplitude A_{sp} is reduced (the lateral scale is 150 nm). Region A corresponds to non-contact mode where the topography of the liquid on the stripes can be discerned. In region B A_{sp} is reduced, inducing a transition to tapping mode and subsequent loss of liquid topography and a negative "phase jump" . The phase also assumes positive values on the carboxylic stripes (cross-section 2). In region C the original non-contact mode is restored.

Fig. 3b where the constant phase value in region A has been arbitrarily set to zero as a reference.

It is also apparent that the phase is not uniform all over the region B. On the carboxylic stripes the phase assumes large positive values (see cross-section 2). This behavior can be explained as the effect of large attractive forces acting on the tip while crossing the liquid stripes. In fact, the adhesion energy between the silicon oxide tip and the substrate is larger on the carboxylic-terminated regions compared to the methyl-terminated surface [32]. Further, the tip experiences capillary forces on the COOH stripes due to the presence of the ethanol wetting film. Both these attractive interactions may dominate the repulsive contact interaction, thus increasing the phase lag of the cantilever [31]. A similar behavior has been observed by Haugstad and Jones while imaging thin polyvinyl alcohol films drop cast on mica [33]. These observations indicate that stable profiles of the liquid structures can only be obtained in the non-contact regime and that a transition of the cantilever to the tapping mode leads to substantial perturbation of the liquid surface and consequently topography artifacts.

The condensation of ethanol on a regular array of 150 nm wide, parallel nanostripes separated by 80 nm, has also been investigated with non-contact mode at several sample temperatures. Representative AFM images are shown in Fig. 4 corresponding to ΔT equal to (a) 10 °C, (b) 0.5 °C and (c) −15 °C. The corresponding transverse profile shapes are shown in Fig. 4d. In (a), corresponding to the largest positive ΔT, only a small amount of liquid is condensed on the stripes and the substrate is relatively dry (Fig. 4a,d solid line). This image also indicates that the chemical stripes have only a minimal positive topographical contrast (∼4 Å) compared to the neighboring methyl terminated regions. This height difference is likely due to a single monolayer of ethanol adsorbed on the stripes. When the temperature offset is reduced to $\Delta T = 0.5$ °C, close to saturation, the liquid condensation is clearly visible on the stripes and the thin liquid film (2.6 nm thick) is nearly

uniform across the stripe (Fig. 4b,d dotted line). In the over-saturated case ($\Delta T = -15$ °C) the amount of liquid condensed on the stripes is even greater and now the liquid topography appears curved with a cylindrical-like topographical profile (Fig. 4c,d dashed line). The process is completely reversible and it is possible to nearly dry the stripes by heating the substrate up to $\Delta T = 10$ °C.

These images clearly demonstrate that the ethanol totally wets the COOH terminated lines but it does not wet the regions terminated by the methyl groups. The apparent contact angle at the stripe's boundary, determined by fitting a circle to the data (see Fig. 4d), was found to be $12 \pm 1°$. This value is considerably less than the advancing contact angle on a uniform OTS surfaces ($30 \pm 1°$ as measured optically on millimeter-sized drops of ethanol) and this explains why the liquid stays confined to the COOH terminated lines. Spill-over into the methyl terminated spacers between the lines should occur only at sufficiently large negative ΔT when the contact angle exceeds the 30° limit. At this point, two adjacent channels can bridge together forming one larger channel and this corresponds to the "morphological wetting transition" discussed by Lenz and Lipowsky [19].

For ethanol, the bridging morphological wetting transition occurs during the over-saturated regime for very large and negative ΔT. This regime could not be explored with our experimental configuration. Therefore, we have investigated the morphological wetting transition for octane where the measured contact angle on an OTS surface is $8 \pm 1°$ rather than the $30 \pm 1°$ observed for ethanol. Thus, a much smaller negative ΔT is required to induce the liquid to spill-over the chemically patterned lines and bridge with neighboring lines. An example of this bridging phenomenon is shown in Fig. 5a,b. Here the pattern is composed of pairs of parallel stripes with variable spacing. Initially (a) the octane condenses only on the stripes but when ΔT is sufficiently negative the liquid spills over the stripes and bridging occurs for the three most closely spaced lines (b).
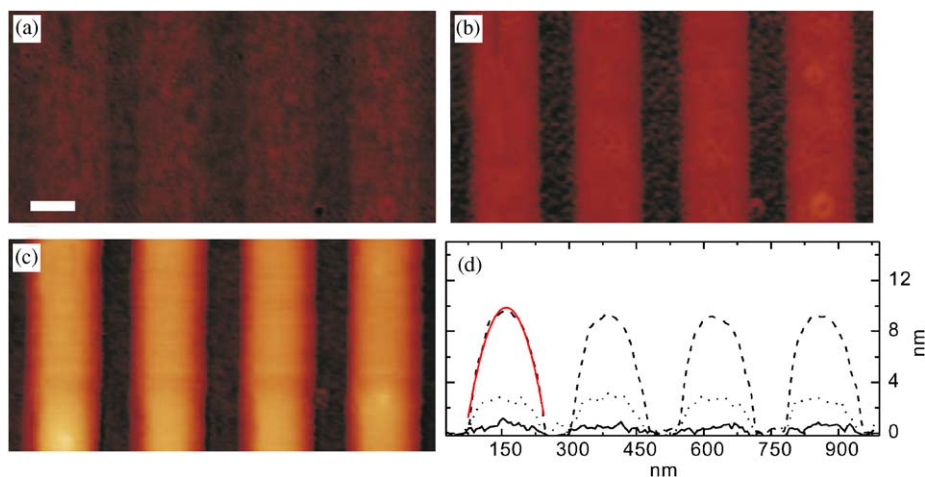
Fig. 4. Condensation of ethanol onto COOH nanostripes for ΔT equal to: (a) $10\,°C$; (b) $0.5\,°C$ and (c) $-15\,°C$ (lateral scale is $100\,nm$). (d) Cross-sectional profiles corresponding to (a) (solid line), (b) (dotted line) and (c) (dashed line). A circle (solid line) has been fitted to a "liquid stripe" of (c).
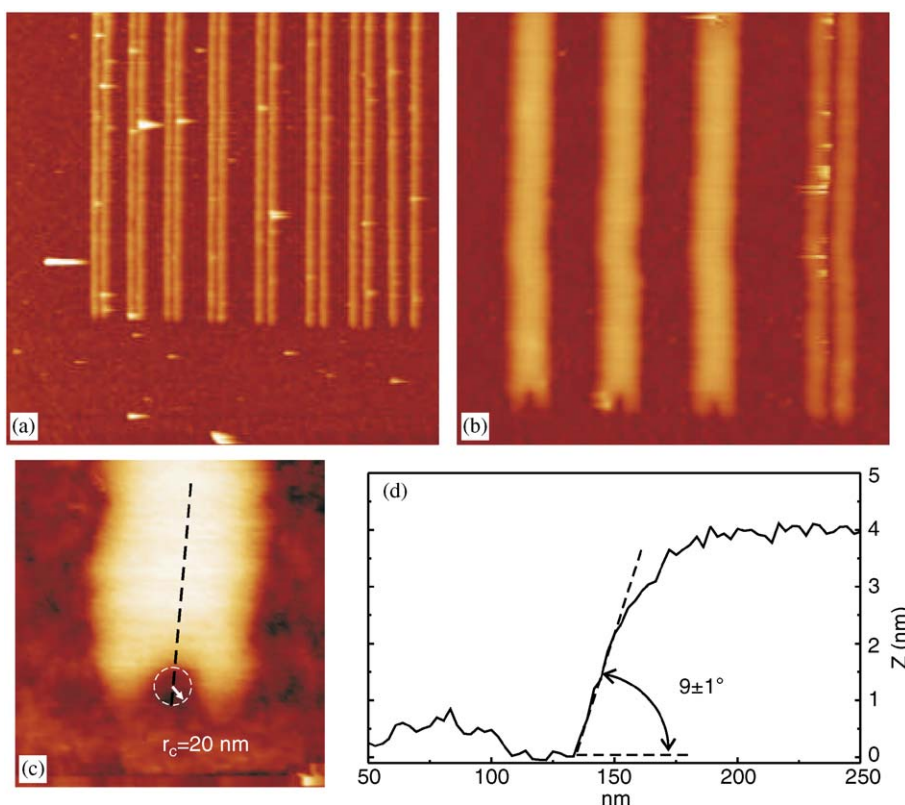

Fig. 5. (a) Octane condensation on pairs of single COOH terminated lines; (b) bridging of the most closely spaced lines and (c) detail of the region at the end of the lines and estimated curvature of the contact line on the methyl surface between the COOH stripes. (d) Liquid profile across the dotted line on (c) where the measured contact angle is $\theta_{r_c} = 9 \pm 1°$ at the non-wetting methyl surface.

This result suggests that by adjusting the sample temperature, and therefore the amount of liquid condensed on the sample, nanoscale morphological wetting transitions can be investigated.

The liquid morphology at the region at the end of two bridged lines, enlarged in Fig. 5c, exhibits characteristics which shed light on the value of the line tension. This image, acquired with the HiRes tips, shows details with lateral resolution better than $10\,nm$. The octane contact line is clearly curved in the methyl region between the two lines. This has occurred since the contact angle of the liquid on the methyl surface is non-zero and the liquid slightly dewets locally to minimize its total interfacial energy. The contact line curvature, at the ends of the line segments about halfway between the closely spaced lines, was estimated by extracting the contact line shown in Fig. 5c and by fitting a circle to it. This gave a local curvature radius $r_c = 20 \pm 5\,nm$. The apparent contact angle of the

liquid in the same region was measured by taking a cross section profile halfway between the stripes (dotted line in Fig. 5c) which is shown in Fig. 5d. The contact angle was found to be $\theta_{r_c} = 9 \pm 1°$. The error is mainly due to the tip/sample convolution artifact and it has been estimated through deconvolution [34] of the image in Fig. 5c. This error is small because of the sharp tips used and the small aspect ratio of the liquid structure. θ_{r_c} is very similar to $\theta_\infty = 8 \pm 1°$, the contact angle of larger octane drops on the OTS surface. We would expect that, due to the line tension τ [10], θ_{r_c} differs from the macroscopic Young's angle, θ_∞.

In first approximation θ_{r_c} is given by the "Modified Young's Equation" [10]:

$$\cos \theta_{r_c} = \cos \theta_\infty - \frac{\tau}{\gamma} \frac{1}{r_c}, \tag{1}$$

where γ is the liquid surface tension. A more precise form of Eq. (1) includes corrections due to the high curvature of the contact line [35,36]. By using Eq. (1) and the experimental values reported above we arrive at a value for the line tension of $\tau = -1 \pm 2 \times 10^{-12}$ J/m which is in agreement with estimations based on recent theoretical models [10]. Additional measurements for a range of r_c would provide a better measure of τ with a smaller uncertainty. Nevertheless, it is evident that the chemical nanopatterns used here provide a unique opportunity to measure the expected weak line tension of liquids. In the past, chemical patterns obtained with the so called "microcontact printing" technique [37] have been used for the same purpose [17], albeit with much larger features. Nevertheless, the patterning method used here also represents a considerable improvement in terms of chemical homogeneity and absence of topographical contrast. This is critical because chemical and physical heterogeneities of the solid surface are known to have a dramatic effect on the wettability and this may strongly affect the value of the measured line tension [10].

4. Conclusion and summary

This work demonstrates that static liquid structures condensed from the vapor phase onto chemical nanopatterns can be imaged using non-contact mode AFM. This gentle profiling mode minimizes the perturbation of the liquid interface in comparison to the tapping regime which occurs at high oscillator amplitudes. A lateral resolutions better than 10 nm can be achieved by using cantilever tips with a very small radii of curvature and this permits studies of nanometer-sized liquid morphologies. The ability to precisely control the amount of liquid condensed on a chemical nanopattern of arbitrary geometry makes it possible to study a large variety of morphological wetting transitions. In particular, we have shown that a geometry composed of alternating wettable/non-wettable nanostripes can induce strong curvatures of the contact line (in the range of 10 nm). In this case the dependence of the local contact angle on the contact line curvature, due to the line tension, can be more accurately ascertained.

References

[1] S. Magonov, V. Elings, M.-H. Whangbo, Surf. Sci. 375 (1997) L385.
[2] G. Bar, Y. Thomann, M.-H. Whangbo, Langmuir 14 (1998) 1219.
[3] D. Anselmetti, R. Lüthi, E. Meyer, T. Richmond, M. Dreier, J. Frommer, H.-J. Güntherodt, Nanotechnology 5 (1994) 87.
[4] C. Bustamante, D. Keller, Phys. Today 48 (1995) 33.
[5] S. Lindsay, The scanning probe microscopy in biology, in: Scanning Probe Microscopy and Spectroscopy: Theory, Techniques, and Applications, second edition, Wiley, New York, 2000.
[6] J. Hu, X.-D. Xiao, D. Ogletree, M. Salmeron, Science 268 (1995) 267.
[7] J. Hu, X. Xiao, M. Salmeron, Appl. Phys. Lett. 67 (1995) 476.
[8] M. Luna, J. Colchero, A.M. Baró, J. Phys. Chem. B 103 (44) (1999) 9576.
[9] A. Gil, J. Colchero, M. Luna, J. Gómez-Herrero, A.M. Baró, Langmuir 16 (2000) 5086.
[10] A. Checco, J. Daillant, P. Guenoun, Phys. Rev. Lett. 91 (2003) 186101.
[11] A. Checco, H. Schollmeyer, R. Boukherroub, J. Daillant, P. Guenoun, Langmuir 22 (2006) 116.
[12] S. Herminghaus, A. Fery, D. Reims, Ultramicroscopy 69 (1997) 211.
[13] R. Garcia, R. Perez, Surf. Sci. Rep. 47 (2002) 197.
[14] J. Tamayo, R. Garcia, Langmuir 12 (1996) 4430.
[15] L. Zitzler, S. Herminghaus, F. Mugele, Phys. Rev. B 66 (2002) 155436.
[16] R. Seemann, M. Brinkmann, E. Kramer, F. Lange, R. Lipowsky, Proc. Natl. Acad. Sci. USA 102 (2005) 1848.
[17] T. Pompe, S. Herminghaus, Phys. Rev. Lett. 85 (2000) 1930.
[18] J. Eijkel, A. van den Berg, Microfluidics Nanofluidics 1 (2005) 249.
[19] P. Lenz, R. Lipowsky, Phys. Rev. Lett. 80 (1998) 1920.
[20] M. Brinkmann, R. Lipowsky, J. Appl. Phys. 92 (2002) 4296.
[21] C. Bauer, S. Dietrich, Phys. Rev. E 61 (2000) 1664.
[23] R. Maoz, S. Cohen, J. Sagiv, Adv. Mater. 11 (1999) 55.
[24] Y. Cai, A. Checco, O. Gang, B. Ocko, in preparation.
[25] A. Noy, C. Sanders, D. Vezenov, S. Wong, C. Lieber, Langmuir 14 (1998) 1508.
[26] C. Bain, E. Troughton, Y.T. Tao, J. Evall, G. Whitesides, R. Nuzzo, J. Am. Chem. Soc. 111 (1989) 321.
[27] U. Hartmann, Ultramicroscopy 85 (1992) 1930.
[28] B. Anczykowski, D. Krüger, H. Fuchs, Phys. Rev. B 53 (1996) 15485.
[29] A. Kühle, A.H. Sørensen, J. Bohr, J. Appl. Phys. 81 (1997) 6562.
[30] L. Nony, R. Boisgard, J.-P. Aimé, J. Chem. Phys. 111 (1999) 1615.
[31] R. García, A.S. Paulo, Phys. Rev. B 60 (1999) 4961.
[32] G. Bar, S. Rubin, A. Parikh, B. Swanson, T.J. Zawodzinski, M.-H. Whangbo, Langmuir 13 (1997) 373.
[33] G. Haugstad, R. Jones, Ultramicroscopy 76 (1999) 77.
[34] D. Keller, Surf. Sci. 253 (1991) 353.
[35] H. Dobbs, Int. J. Mod. Phys. B 13 (1999) 3255.
[36] C. Bauer, S. Dietrich, Phys. Rev. E 62 (2000) 2428.
[37] A. Kumar, G. Whitesides, Appl. Phys. Lett. 63 (1993) 2002.
[38] A. Checco, O. Gang, B.M. Ocko, Phys. Rev. Lett. 96 (2006) 056104.
[39] D. Wouters, R. Willems, S. Hoeppener, C.F.J. Flipse, U.S. Schubert, Adv. Funct. Mater. 22 (2005) 938.